2019 American Control Conference (ACC)
Philadelphia, PA, USA, July 10-12, 2019

Hybrid Integral Reset Control with Application to a Lens Motion System

K.G.J.Gruntjens M.F.Heertjes S.J.L.M.van Loon N.van de Wouw W.P.M.H.Heemels

***Abstract*— A hybrid integral controller with reset is proposed. This hybrid controller ensures improved low-frequency disturbance rejection properties under double integrator (PI^{2}D) control without inducing the undesired increase of overshoot otherwise resulting from adding an extra linear integrator to a PID controller. The controller is applied to an optical lens motion system that requires PID control in one operating mode and PI^{2}D control in the other, therewith motivating a hybrid integral control strategy. The reset element in the controller is included to improve transient performance. To guarantee closed-loop stability, a conditional (and partial) reset rule is introduced that restricts the input-output behavior of the dynamic reset element, *i.e.*, the hybrid integrator with reset, to a bounded sector. As a result, stability can be guaranteed on the basis of a circle criterion-like argument and checked by (measured) frequency response data. Stability and performance of the hybrid integral control design with conditional (and partial) reset are investigated by application to a piezo-actuated lens system that is part of an industrial wafer scanner.**

***Index Terms*— circle criterion, hybrid control, Lyapunov stability, motion systems, reset control, wafer scanners.**

I. Introduction

This paper proposes a novel hybrid integral controller design with conditional reset to cope with the conventional tradeoff between (a) improved low-frequency disturbance suppression through integral control and (b) deteriorated transient response due to such integral control. This tradeoff generically arises in high-precision motion control applications such as for example wafer scanners in the lithography industry [9] and robotics [11].

The above-mentioned tradeoff between frequency-domain disturbance rejection properties and time-domain overshoot and settling behavior is well known to the control community [12], [5]. Also, this tradeoff occurs in many linear control problems for a variety of control applications. In an attempt to balance this tradeoff in a more desirable manner, nonlinear control has been opted. A recent advancement is found in [9] that combines a variable-gain integral controller with a Clegg integrator — measurement results obtained from a piezo-actuated lens system demonstrated its benefits. Stability of the reset system essentially required the satisfaction of two conditions: a flow condition in the intervals between resets, and a jump condition at the resets [12].

In this paper, the hybrid (variable-gain) controller from [9] is given additional reset functionality. A key contribution of the current paper lies in the fact that the reset conditions are designed such that the input-output behavior of the reset element belongs to the sector $[0, \alpha]$ with $\alpha > 0$ a positive (finite) gain, see in this regard also [10]. As a result, input-to-state stability of the closed-loop hybrid system with reset can be guaranteed by combining a circle criterion-like argument together with a detectability condition for the reset element; note that the latter includes an integrator, which is not memoryless, and thus requires extra attention beyond the conventional circle criterion arguments. The advantage of such an argument lies in the fact that the stability conditions can be assessed by evaluating (measured) frequency response data of the linear part of the closed-loop system in relation to the (sector) gain α, herewith indeed avoiding the need for a parametric plant model. The adapted reset conditions, however, cause pre-resets that could come at the expense of performance. To limit the possible loss of performance associated to these pre-resets and as a second contribution, a partial integrator reset is proposed, which employs a state-dependent reset map. A third contribution of the paper is the application of the hybrid integral controller with conditional reset to an industrial piezo-actuated lens system of a wafer scanner including real industrial experiments.

The remainder of this paper is organized as follows. In Section II, the lens control problem is discussed in more detail. This forms the motivation for designing the hybrid integral control element with reset in Section III. In Section IV, the circle criterion-like stability argument is presented that results in easy-to-check stability conditions. In Section V, the occurrence of pre-resets is further analyzed along with the measurement results obtained by application of the hybrid control strategy to the piezo-actuated lens system. Section VI summarizes the main conclusions.

II. Lens control problem

Being part of a wafer scanner, active lens elements are used for projecting and re-scaling of the image of the microchip coming from the mask (or reticle) prior to wafer exposure. Each lens element, an example of which is given in Fig. 1, consists of three piezoelectric actuators and three sensors to control the lens in three degrees-of-freedom (DOFs), *i.e.*, translational (z) and two rotational (r_x and r_y) axes. There are basically two types of motion for the driving rod of the piezoelectric actuator to propel along the z-axis, namely:

This research is financially supported by the Dutch Science Foundation STW via the project "Hyper Motion: Hybrid Control for Performance Improvement of Linear Motion Systems" (no. 10953).

K.G.J. Gruntjens is with Demcon, Eindhoven, The Netherlands, email: koen.gruntjens@demcon.nl (during the main execution of this work Koen Gruntjens was with Eindhoven University of Technology and ASML)

M.F. Heertjes is with Eindhoven University of Technology, Department of Mechanical Engineering, Den Dolech 2, 5600 MB Eindhoven, The Netherlands, email: m.f.heertjes@tue.nl. and with ASML Netherlands B.V., Mechatronics System Development, De Run 6501, 5504 DR Veldhoven, The Netherlands, email: marcel.heertjes@asml.com

S.J.L.M. van Loon is with Demcon, Eindhoven, The Netherlands, email: bas.van.loon@demcon.nl (during the main execution of this work Bas van Loon was with Eindhoven University of Technology)

N. van de Wouw is with the Department Mechanical Engineering, Eindhoven University of Technology, Eindhoven, The Netherlands, the Department of Civil, Environmental and Geo-Engineering, University of Minnesota, Minneapolis, MN 55455 USA, and also with the Delft Center for Systems and Control, Delft University of Technology, Delft, The Netherlands (e-mail: n.v.d.wouw@tue.nl).

W.P.M.H. Heemels is with Eindhoven University of Technology, Department of Mechanical Engineering, Control Systems Technology Group, Den Dolech 2, 5600 MB Eindhoven, The Netherlands, email: m.heemels@tue.nl.

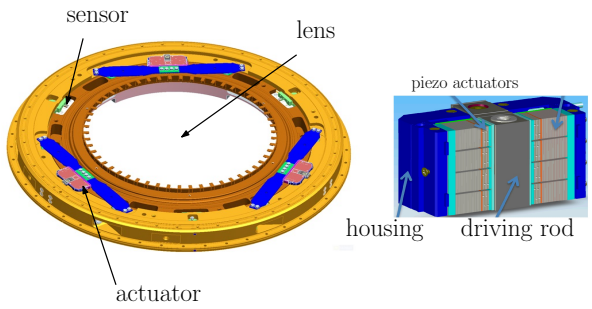

Fig. 1: Example of a lens element and piezoelectric actuator.

1) analogue (scanning) motion during wafer exposure conducted under closed-loop conditions within a limited range of operation, typically ± 2.5 μm, and
2) shuffle motion conducted under open-loop conditions, which is used to recalibrate the actuator and which is called for as soon as the operating limits of the piezo actuators are reached in scanning motion.

Ideally, in shuffle motion the driving rod remains at a fixed position. However, the driving rod is known to drift, which leads to position errors that remain unnoticed – that is to say, until completing the shuffle motion. After shuffle motion and as a result of closing the loop again at the beginning of the scanning motion, the system is exposed to the resulting step disturbance, referred to as a shuffle disturbance. The magnitude behavior of this shuffle disturbance strongly depends on the actuator properties, e.g. material properties, hysteresis, and drift in combination with the power amplifier involved. From a control perspective, it is important to note that these step disturbances (in principle) vary in an *a priori* unknown manner each time a shuffle motion takes place, thereby rendering standard feedforward control solutions ineffective. We approach this problem through (nonlinear) feedback control.

In support of feedback control design, consider the lens system dynamics in $z-$direction as depicted in the Bode diagram of Fig. 2. The figure shows both measured frequency

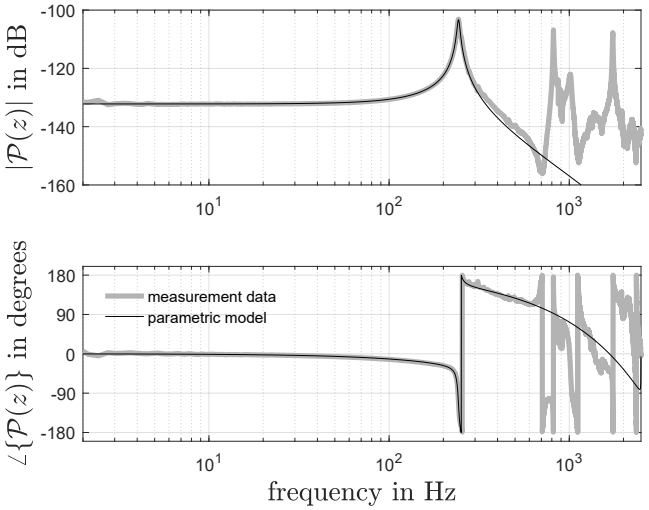

Fig. 2: Bode diagram of a lens system in z-direction: a) FRF measurement data (gray), and b) data from a simple parametric model (black).

response function data and the data obtained from a simple parametric model given by

$$\mathcal{P}(z) = (1 - z^{-1})\mathcal{Z}\left\{\frac{\mathcal{P}(s)}{s}\right\},\ \mathcal{P}(s) = \frac{1}{ms^2 + bs + k}, \tag{1}$$

with $s = j\omega \in \mathbb{C}$ the Laplace variable, $m = 1.75$ kg the lens mass, $b = 95.6$ Ns/m a damping coefficient, $k = 4.1 \cdot 10^6$ N/m a spring constant, and $P(z)$ the result of plant $\mathcal{P}(s)$ in combination with a zero-order-hold circuit, $\mathcal{Z}\{\mathcal{P}(s)/s\}$ denoting the z-transform of the sampled time-series whose Laplace transform is the expression for $\mathcal{P}(s)/s$ with $z^{-1} = e^{sT}$ a unit time delay, and $T = 2 \cdot 10^{-4}$ seconds sampling time.

The lens system is controlled by the nominal LTI controller $\mathcal{C}_{fb}$, or in (continuous-time) transfer function notation

$$\mathcal{C}_{fb}(s) = \mathcal{C}_{pid}(s)\mathcal{C}_{lp}(s)\mathcal{C}_1(s)\mathcal{C}_2(s), \tag{2a}$$

which consists of a proportional-integral-derivative (PID) controller $\mathcal{C}_{pid}$ in series connection to a second-order low-pass filter $\mathcal{C}_{lp}$ and two notch filters $\mathcal{C}_n$ with $n \in \{1, 2\}$, where

$$\mathcal{C}_{pid}(s) = k_p\Big(\frac{s}{\omega_d} + 1 + \frac{\omega_{i,1}}{s}\Big), \tag{2b}$$

$$\mathcal{C}_{lp}(s) = \frac{1}{\Big(\frac{s}{\omega_{lp}}\Big)^2 + 2\zeta_{lp}\Big(\frac{s}{\omega_{lp}}\Big) + 1}, \tag{2c}$$

$$\mathcal{C}_n(s) = \frac{(\omega_n^p)^2}{(\omega_n^z)^2} \cdot \frac{s^2 + 2\zeta_n^z(\omega_n^z)s + (\omega_n^z)^2}{s^2 + 2\zeta_n^p(\omega_n^p)s + (\omega_n^p)^2}. \tag{2d}$$

The corresponding controller parameter values are listed in TABLE I. In addition to the filters in the nominal controller

TABLE I: Controller parameters.

k_p	126600	-	ζ_1^z	0.5	-
f_{i1}	1100	Hz	f_1^p	239	Hz
f_{i2}	12.3	Hz	ζ_1^p	0.1	-
f_d	1e6	Hz	f_2^z	650	Hz
f_{lp}	185	Hz	ζ_2^z	0.5	-
ζ_{lp}	0.85	-	f_2^p	285	Hz
f_{n1z}	239	Hz	ζ_2^p	0.9	-

$\mathcal{C}_{fb}$, a linear lag filter $\mathcal{C}_i$ given by

$$\mathcal{C}_i(s) = \frac{s + \omega_{i,2}}{s}, \tag{3}$$

with $\omega_{i,2}$ the integrator cut-off frequency, can be added in series. This lag filter is employed in the control strategy in the following manner. The lens control system uses control mode switching between two linear controllers: PID $:= \mathcal{C}_{fb}(s)$ in analogue (shuffle) mode, and PI^{2}D $:= \mathcal{C}_i(s)\mathcal{C}_{fb}(s)$ in scanning mode. Both controllers induce roughly the same bandwidths of the closed-loop system of approximately 30 Hz, but significantly differ in terms of low-frequency disturbance rejection properties, the latter being the result of the extra integrator in (3) in the PI^{2}D controller.

III. Hybrid integral reset control design

Consider the hybrid integral control element with reset as shown in Fig. 3, that will serve as a substitute for $\mathcal{C}_i$ in the previous section, *i.e.*, a nonlinear lag filter obtained by

1) a switching element ϕ that multiplies input e with a gain of either 0 or 1 depending on the input magnitude;
2) a reset integrator element that resets its single state upon zero crossings of e;
3) a unity feedthrough path that adds the reset integrator output $-u$ to the initial input signal e resulting in the output signal $w = e - u$.

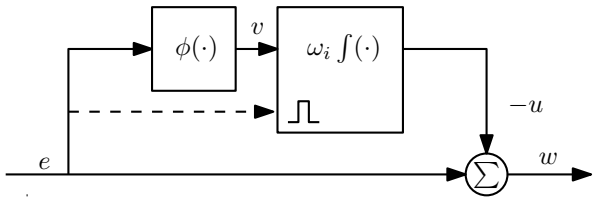

Fig. 3: Schematic representation of the hybrid integral control element with reset, where the dashed line illustrates the reset condition of the reset integrator.

In Fig. 3, the internal signal $v = \phi(e)$ denotes the output of the switching element $\phi(\cdot)$ that is defined as

$$\phi(e) := \begin{cases} e, & \text{if } |e| \leq \delta, \\ 0, & \text{otherwise}, \end{cases} \tag{4}$$

with $\delta > 0$ the switching length. To properly describe the dynamics underlying Fig. 3, consider the following impulsive differential equation (IDE):

$$\begin{cases} \dot{x}_I(t) &= \omega_i v(t), & \text{if } e(t) \neq 0, & \text{(5a)} \\ x_I(t^+) &= \epsilon x_I(t), & \text{if } e(t) = 0, & \text{(5b)} \\ w(t) &= x_I(t) + e(t), & & \text{(5c)} \end{cases}$$

with $x_I(t) \in \mathbb{R}$, with $t \in \mathbb{R}_{\geq 0}$, denoting the integrator state, $x_I(t^+)$ denoting the state directly after a reset (at time t^+) *i.e.*, $x_I(t^+) := \lim_{\tau \to t, \tau > t} x_I(\tau)$, and $0 \leq \epsilon < 1$ giving the portion by which state $x_I(t)$ is reset, for example $\epsilon = 0$ implies $x_I(t^+) = 0$, *i.e.*, a full reset to zero; note that (4) and (5) can be cast in the hybrid forms as given in [1]. In absence of any reset, *i.e.*, when $e(t) \neq 0$, the solutions of (5) evolve conform the flow dynamics (5a) while (5b) denotes the impulsive dynamics (or jump dynamics) being active only at resets, *i.e.*, when $e(t) = 0$. Consider the following two distinctive cases that arise as a result of (4):

1) if $|e(t)| \leq \delta$, (5) is equivalent to

$$\begin{cases} \dot{x}_I(t) &= \omega_i e(t), & \text{if } e(t) \neq 0, \\ x_I(t^+) &= \epsilon x_I(t), & \text{if } e(t) = 0, \\ w(t) &= x_I(t) + e(t), & \end{cases} \tag{6}$$

in which the linear flow dynamics ($e(t) \neq 0$) are represented by the transfer function

$$\frac{w(s)}{e(s)} = \frac{s + \omega_i}{s}, \text{ if } 0 < |e(t)| \leq \delta; \tag{7}$$

2) if $|e(t)| > \delta$, then $\phi(e(t)) = v(t) = 0$ and the reset integrator maintains a constant buffer load $-u_c = -u(\tau)$ with τ the last time instant satisfying $|e(\tau)| = \delta$; when $|e(t)| \gg \delta$, u_c often becomes negligible with respect to e, *i.e.*, $w(s)/e(s) \approx 1$.

IV. Stability conditions with conditional and partial reset

Consider the hybrid integral reset control system in Fig. 4, where the nonlinear elements, *i.e.*, the switching element $\phi(\cdot)$ and the reset integrator both captured in $\mathcal{R}$, are being isolated from the linear dynamics represented by $\mathcal{H}$. In the figure, r

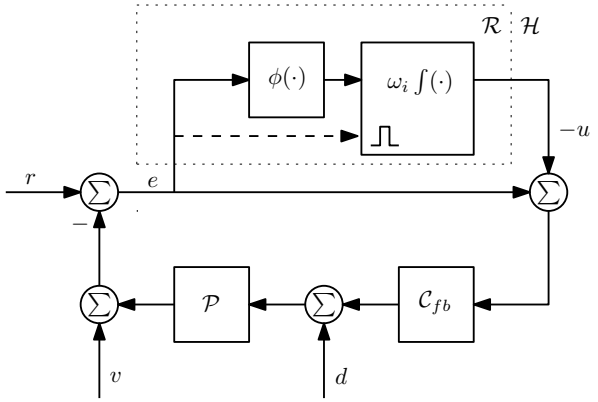

Fig. 4: Simplified schematics of a closed-loop hybrid integral reset control system.

represents the reference to be tracked, e is a closed-loop error signal, $\mathcal{C}_{fb}$ the nominal PID-based feedback controller, d a force disturbance, $\mathcal{P}$ the plant, and ν the output disturbance, *e.g.*, sensor noise.

To obtain stability conditions that allow for verification on the basis of frequency response data, the closed-loop system is transformed into a Lur'e-type system, see Fig. 5. Note that the essential difference with a (true) Lur'e-type system lies in the fact that we consider a *dynamical* nonlinear system $\mathcal{R}$ — $\mathcal{R}$ contains an integrator — rather than a memoryless nonlinearity.

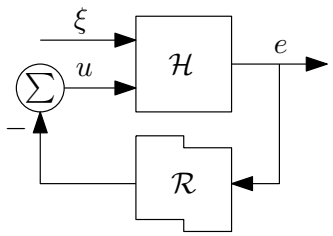

Fig. 5: Lur'e-type system representation.

A. Closed-loop system representation

Consider Fig. 5 where $\mathcal{H}$ represents a continuous-time LTI dynamical system that in state-space description reads

$$\mathcal{H} : \begin{cases} \dot{x}_h(t) &= Ax_h(t) + Bu(t) + B_\xi \xi(t) \\ e(t) &= Cx_h(t) + D_\xi \xi(t), \end{cases} \tag{8}$$

with $e(t), u(t) \in \mathbb{R}$, and $x_h(t) \in \mathbb{R}^{n_h}$ the state vector containing the (physical) states of plant $\mathcal{P}$ and feedback controller $\mathcal{C}_{fb}$ in Fig. 4 at time $t \in \mathbb{R}_{\geq 0}$. Moreover, $\xi(t) = [r(t) \;\; d(t) \;\; \nu(t)]^T \in \mathbb{R}^3$ denotes the augmented input vector, and (A, B, C) is assumed to correspond to a minimal realization. The transfer function between input $u(s)$

and output $e(s)$ of (8) equals the complementary sensitivity function $\mathcal{G}_{eu}(s)$, which is given by

$$\begin{aligned}\mathcal{G}_{eu}(s) &:= C(sI-A)^{-1}B \\ &= \frac{\mathcal{P}(s)\mathcal{C}_{fb}(s)}{1+\mathcal{P}(s)\mathcal{C}_{fb}(s)}.\end{aligned} \tag{9}$$

Consider the nonlinear dynamical system $\mathcal{R}$ with input-output pair $(e,-u)$ which consists of the cascaded connection of the switching element $\phi(\cdot)$ in (4) and the reset integrator dynamics in (5) without feedthrough term and which further differs from (5) in terms of defining the reset conditions. As a result, $\mathcal{R}$ is given by the following IDE,

$$\mathcal{R}: \begin{cases} \dot{x}_I(t) & = \begin{cases}\omega_i e(t), & \text{if } |e(t)| \le \delta \\ 0, & \text{otherwise}\end{cases}, \text{ if } (e,-u)\in\mathcal{F}, \\ x_I(t^+) & = \epsilon x_I(t), \qquad\qquad \text{if } (e,-u)\in\mathcal{J}, \\ -u(t) & = x_I(t), \end{cases} \tag{10}$$

see also (4) and (5). Note that the conditional and partial reset condition is defined via the flow set $\mathcal{F}$ and the jump set $\mathcal{J}$, see also [8] for more details. As such, system $\mathcal{R}$ behaves continuously conform the differential equation in (10) as long as $(e,-u)\in\mathcal{F}$, hence the input-output pair $(e,-u)$ satisfies the condition $eu \le -u^2/\alpha$, whereas state x_I will jump instantaneously from x_I to $x_I^+ = \epsilon x_I$ when $(e,-u)\in\mathcal{J}$. Now let us define the flow set $\mathcal{F}$ and the jump set $\mathcal{J}$ according to

$$\begin{aligned}\mathcal{F} &:= \{(e,-u)\in\mathbb{R}^2 \mid eu \le -\frac{1}{\alpha}u^2\}, \\ \mathcal{J} &:= \{(e,-u)\in\mathbb{R}^2 \mid eu \ge -\frac{1}{\alpha}u^2\},\end{aligned} \tag{11}$$

with $\alpha\in\mathbb{R}_{>0}$. Given (11), the input-output pair $(e,-u)$ of (10) is (apart from a possible initial condition) restricted to the sector $[0,\ \alpha]$ as illustrated by Fig. 6.

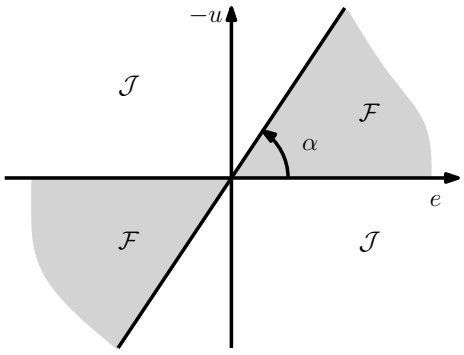

Fig. 6: Graphical representation of the flow set $\mathcal{F}$ and the jump set $\mathcal{J}$ as defined in (11).

Remark 1 *According to the framework in [12], the nonlinear system $\mathcal{R}$ in* (10)*, i.e., the hybrid integral controller with conditional reset, for increasing α tends to the original hybrid integral controller with reset in* (5)*, for which the input-output pair $(e,-u)\in\mathbb{R}^2$ lies in the sector $[0,\ \infty)$.*

B. Closed-loop Stability

Consider the closed-loop system in Fig. 5 with the corresponding state vector $x(t) := [x_I(t)\ x_h^T(t)]^T \in \mathbb{R}^n$ at time $t\in\mathbb{R}_{\ge 0}$ in which $x_I(t)\in\mathbb{R}$ is governed by (10), (11) and $x_h(t)\in\mathbb{R}^{n_h}$ consists of both the states of plant $\mathcal{P}$ in (1) as well as the states of $\mathcal{C}_{fb}$ in (2) and is governed by (8).

Definition 1 *The closed-loop hybrid system in* (8) *with* (10) *is said to be pre-input-to-state stable (pre-ISS) if there exist a $\mathcal{KL}$-function β and $\mathcal{K}$-function γ such that for any solution pair (x,ξ) to* (8)*,* (10) *with $\xi\in\mathcal{L}_\infty$ it holds that*

$$||x(t)|| \le \max\left\{\beta(||x(0)||,t), \gamma(||\xi||_\infty)\right\}, \forall t \in \textit{dom } x, \tag{12}$$

in which (for simplicity of presentation) we did not use the hybrid system notation of [8]. In (12), the effect of the initial conditions (for zero input $r(t)=\nu(t)=d(t)=0$) eventually fades away. For non-zero input $\xi\neq 0$, multiple steady-state solutions may occur within the compact (and invariant) set which is characterized by γ.

The following result poses sufficient conditions under which pre-ISS of the closed-loop system (8), (10), (11) in Fig. 5 can be guaranteed.

Theorem IV.1 *Consider the closed-loop hybrid system with conditional reset as in Fig. 5 with $\mathcal{H}$ as in* (8) *and $\mathcal{R}$ as in* (10)*,* (11) *and fixed $\alpha\in(0,\infty)$. Then, the closed-loop system is pre-ISS according to Definition 1 if the following conditions are satisfied:*

$$(a)\quad \mathcal{G}_{eu}(j\omega) \textit{ in } (9) \textit{ is Hurwitz}, \tag{13a}$$

$$(b)\quad Re\{\mathcal{G}_{eu}(j\omega)\} > -\frac{1}{\alpha}, \textit{ for all } \omega\in[-\infty,\infty]. \tag{13b}$$

Proof: We call a smooth function $W:\mathbb{R}^{n_h+1}\to\mathbb{R}$ an ISS-Lyapunov (ISSLF) function, see [6], for the system (8) with (10) and (11), if it satisfies, for $\kappa_j>0$, $j\in\{1,2,3,4\}$, the conditions

$$\kappa_1\|x\|^2 \le W(x) \le \kappa_2\|x\|^2, \qquad \text{for all } x\in\mathbb{R}, \tag{14a}$$

$$\dot{W}(x) \le -\kappa_3\|x\|^2 + \kappa_4\|\xi\|^2, \quad \text{for all } (e,-u)\in\mathcal{F}, \tag{14b}$$

$$W(x^+) \le W(x), \qquad \text{for all } (e,-u)\in\mathcal{J}. \tag{14c}$$

The existence of such a function W (under the hypothesis of the theorem) can be proved by the following four steps:

- Step 1: initially disregard the internal (nonlinear) dynamics of $\mathcal{R}$ and exploit the fact that the input/output pairs $(e,-u)$ of $\mathcal{R}$ satisfy the sector condition $eu \le -u^2/\alpha$ (possibly after an initial jump) by the grace of the form of $\mathcal{F}$ and $\mathcal{J}$ in (11). Introduce the following auxiliary system (called base nonlinear system)

$$\Sigma_{bns}: \begin{cases}\mathcal{H}: \begin{cases}\dot{x}_h = Ax_h + Bu + B_\xi\xi \\ e = Cx_h + D_\xi\xi\end{cases} \\ u = -\varphi(e),\end{cases} \tag{15}$$

  in which the memoryless nonlinearity $\varphi(\cdot)$ satisfies the sector condition

$$0 \le \varphi(e) \le \alpha e, \tag{16}$$

for all $e \in \mathbb{R}$; the circle criterion can be used to prove that the system Σ_{bns} admits a quadratic ISSLF $V : \mathbb{R}^{n_h} \to \mathbb{R}$;
- Step 2: use a detectability condition on the state of $\mathcal{R}$ to construct a Lyapunov-like function $V_r : \mathbb{R} \to \mathbb{R}$ for the system $\mathcal{R}$ during flow, *i.e.*, for $(e, -u) \in \mathcal{F}$;
- Step 3: show that the functions V of Step 1 and V_r of Step 2 can be combined into a function $W : \mathbb{R}^{n_h+1} \to \mathbb{R}$, satisfying (14a) and (14b) for the total system combining $\mathcal{H}$ and $\mathcal{R}$;
- Step 4: show that W constructed in Step 3 does not increase during resets, thereby also satisfying the ISSLF condition during jumps, *i.e.*, (14c); combining the results of Step 3 and Step 4 (under the consideration of persistently flowing trajectories) allows for construction of a bound on the norm of the total state as in (12) thereby establishing ISS. □

Note that these steps are in line with the steps introduced in [10] with the difference that [10] does not consider the presence of the memoryless nonlinearity $\varphi(\cdot)$. Including $\varphi(\cdot)$ requires exploiting the sector-condition $||u|| \leq \alpha||e||$, which is a mere technicality in the presentation of [10], and which is left to the reader in view of space considerations.

V. Application to a Lens Motion System

In this section, we will further analyze the reset integrator with conditional (and partial) reset as proposed in (10), (11) where we will demonstrate the occurrence of so-called pre-resets. The performance of different reset control variants is subsequently studied through measurement results.

A. The occurrence of pre-resets

Regarding the hybrid integral reset controller with conditional reset, it is important to realize that the introduction of α, *i.e.*, by modifying the reset conditions through re-defining the flow set $\mathcal{F}$ and the jump set $\mathcal{J}$ in (11), may jeopardize the effectiveness of the PI^{2}D-based reset control design. In order to clarify this statement, consider a single (conditional) reset integrator given by the following IDE

$$\tilde{\mathcal{R}} : \begin{cases} \dot{x}_I(t) & = \omega_i e(t), & \text{if } (e,-u) \in \mathcal{F}, \\ x_I(t^+) & = 0, & \text{if } (e,-u) \in \mathcal{J}, \\ -u(t) & = x_I(t). \end{cases} \tag{17}$$

Note that (17) resembles the case of (10) where $|e(t)| \leq \delta$ and $\epsilon = 0$. The flow set $\mathcal{F}$ and the jump set $\mathcal{J}$ are defined as in (11). Let e be a sinusoidal input signal given by

$$e(\tau) = \hat{e}\sin(\tau), \tag{18}$$

with $\tau = \omega t$, $t \in \mathbb{R}_{\geq 0}$ and suppose $x(0)$ is chosen such that $(e, -u) \in \mathcal{F}$. By forward integration using (17), it follows that the output signal u initially evolves according to

$$-u(\tau) = \frac{\omega_i}{\omega}\hat{e}\Big(1 - \cos(\tau)\Big), \tag{19}$$

which is shown in Fig. 7 (thick black curve). Note that on the interval $[0,\ \pi]$, the first reset instant γ follows from

$$e(\gamma) = -\frac{1}{\alpha}u(\gamma), \tag{20}$$

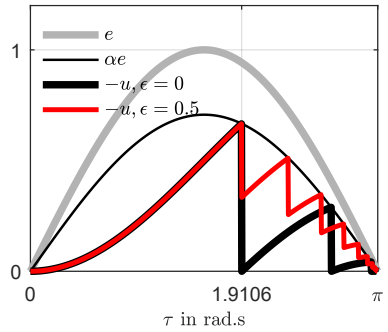

Fig. 7: Response $-u(\tau)$ of the single reset integrator in (23) for a given sinusoidal input signal $e(\tau) = \hat{e}\sin(\tau)$ with $\alpha = \sqrt{1/2}$, $\omega = \omega_i = 3$ rad/s, and $\epsilon \in \{0, 0.7\}$.

which occurs at $\gamma = 1.9106$. Namely, substituting (18) and (19) in (20) gives

$$\sin(\gamma) = \frac{\omega_i}{\alpha\omega}\Big(1 - \cos(\tau)\Big), \tag{21}$$

which, using the trigonometric identity $1 - \cos(\gamma) = 2\sin^2(\gamma/2)$, defining $\nu := \gamma/2$, and after some algebra, gives

$$\gamma = 2\tan^{-1}\left(\frac{\alpha\omega}{\omega_i}\right), \tag{22}$$

hence an explicit relation between α and the reset instances is obtained. By increasing α, (17) increasingly resembles the Clegg integrator with reset condition $eu \leq 0$. On the one hand, lowering α has the positive effect of relaxing the stability requirements but, on the other hand, entails additional pre-resets that may jeopardize the effectiveness of the integrator in achieving performance. In fact, each jump, which corresponds to emptying the integrator buffer, temporary reduces the control force, *i.e.*, temporary reduces the ability of the controller to deal with position error.

To address this tradeoff in an alternative manner, we combine the effect of pre-resetting (with the aim of inducing favorable stability properties) with only partial resetting of the integrator state x_I, through an appropriate choice of the reset portion $0 < \epsilon \leq 1$, hence lower the resulting performance penalty by admitting a post-reset integrator buffer. For the purpose of illustration, consider the IDE

$$\bar{\mathcal{R}} : \begin{cases} \dot{x}_I(t) & = \omega_i e(t), & \text{if } (e,u) \in \mathcal{F}, \\ x_I(t^+) & = \epsilon x_I(t), & \text{if } (e,u) \in \mathcal{J}, \\ -u(t) & = x_I(t), \end{cases} \tag{23}$$

which refers to the case of (10) with $|e(t)| \leq \delta$ and which differs from (17) in the sense that it includes the state-dependent reset map $x_I(t^+) = \epsilon x_I(t)$ with $\epsilon \neq 0$. Consider again the sinusoidal input signal e from (18). By forward integration using (23), the resulting output response $-u$ is depicted in Fig. 7 (thick red curve). Note that $\epsilon = 0.5$ (dashed red curve) gives more staircase-like reset behavior with multiple smaller pre-resets in comparison with the full pre-resets for the case that $\epsilon = 0$ (thin black curve). Also note that partial reset of the conditional integrator in (10), as opposed to partial reset of the unconditional system in (4) and (5) renders the same sign between the input signal e and the output signal $-u$. We therefore expect to lower the performance penalty by keeping a larger integrator buffer.

B. Measurement results

For the lens control system of an industrial wafer scanner, Fig. 8 shows the result of time-series measurements for both scanning (left part) and shuffle motion (right part) when applying the hybrid integral controller with (conditional) reset in (10), (11). It can be seen that for the cases $\alpha = 2.17$

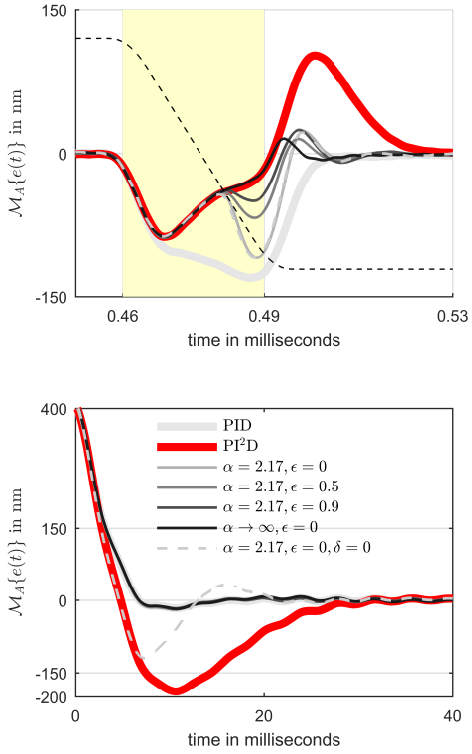

Fig. 8: $\mathcal{M}_A$-filtered error responses $e(t)$ obtained by measurement during: (a) scanning motion with reference signal r (dashed curve, left part), or (b) shuffle motion (right part); $\alpha = \{2.17, 1000\}$, $\delta \in \{0, 150\}$ nm, and $\epsilon \in \{0, 0.5, 0.9\}$.

and $\epsilon \in \{0.5, 0.9\}$, the integrator output largely preserves the integrator buffer during the critical scanning time interval, while this buffer is being emptied in a step-wise fashion mostly during the (non-critical) preparation interval, *i.e.*, from $t = 0.49$ to $t = 0.53$ seconds. As a result, the error responses in scanning motion (left part of the figure) suffer less from the conditional reset law (compare the responses for example with the response obtained with $\alpha = 2.17, \epsilon = 0$, which belongs to the hybrid integral controller with full conditional reset) and demonstrate improved scanning performance compared to PID control. Note that the best performance is still obtained with the unconditional reset law, that is with $\alpha \to \infty$ (in this case $\alpha = 1000$), but without having guarantees on stability through the circle criterion-like conditions from Theorem IV.1, recall also Fig. 2. In terms of shuffle motion (right part of the figure) none of the responses obtained with the conditional reset rule show significant differences with the response obtained from PID control. This is because with the hybrid integral controller with conditional reset, the integrator can only build-up buffer upon entering the interval $e \in [-\delta, \delta]$, which in the experiment is chosen at $\delta = 150$ nm, and which reflects a relatively short time interval. Hence, all responses have less overshoot and settle significantly faster compared to the responses induced by (linear) PI^{2}D control. Performance is also improved in comparison with the responses discussed in [10], *i.e.*, the case of conditional reset without using the switching element such as introduced in (4). This is shown in Fig. 8 by the response indicated with $\delta = 0$, $\alpha = 2.17$, and $\epsilon = 0$. In absence of a switching element ($\delta = 0$ in (4)), it can be seen that the overshoot increases from roughly 18 to 117 nanometer, whereas settling times increase from 13.9 to 21.5 milliseconds.

VI. CONCLUSIONS

This paper proposed a hybrid integral controller with a conditional reset and a state-dependent reset map. The merits of this novel control design when compared to control designs with linear integrators are illustrated by application to an industrial lens motion system such as used in wafer scanners. The hybrid controller is designed to combine the benefit of PI^{2}D control for low-frequency tracking performance with the benefit of PID control for transient performance. Restricting the input-output pair $(e, -u)$ to the sector $[0, \alpha]$, though this allows for the considered (and highly-valued) frequency-domain approach, may induce conservativeness by neglecting the implicit integrator dynamics. Future work should focus on deriving less conservative stability conditions that lead to reduced penalties on closed-loop performance of reset-based control systems.

REFERENCES

[1] M. Al Janaideh, R. Naldi, L. Marconi, and P. Krejčí. (2012) A hybrid system for a class of hysteresis nonlinearity: modeling and compensation. In Proc. Conference on Decision and Control, Maui, Hawaii, pp. 5380–5385.

[2] M. Arcak, M. Larsen, and P. Kokotovic. (2003) Circle and Popov criteria as tools for nonlinear feedback design, Automatica, 39(4), pp. 643-650.

[3] A. Baños, J. Carrasco, and A Barreiro. (2011) Reset times-dependent stability of reset control systems, IEEE Trans. on Automatic Control, 56(1), pp. 217-223.

[4] O. Beker, C.V. Hollot, Y. Chait, and H. Han. (2004) Fundamental properties of reset control systems, Automatica, 40(6), pp. 905-915.

[5] L. Chen, N. Saikumar, S. Baldi, and S.H. Hosseinnia. (2018) Beyond the Waterbed Effect: Development of Fractional Order CRONE Control with Non-Linear Reset. In Proc. American Control Conference, Milwaukee, WI, pp. 545-552.

[6] C. Cai and A.R. Teel. (2009) Characterizations of input-to-state stability for hybrid systems, Systems & Control Letters, 58(1), pp. 47–53.

[7] F. Forni, D. Nesic, and L. Zaccarian. (2011) Reset passivation of nonlinear controllers via a suitable time-regular reset map, Automatica, 47(9), pp. 2099-2106.

[8] R. Goebel, R.G. Sanfelice, and A.R. Teel. (2012) Hybrid dynamical systems: modeling, stability and robustness, Princeton Univeristy Press.

[9] M.F. Heertjes, K.G.J. Gruntjens, S.J.L.M. van Loon, N. Kontaras, and W.P.M.H. Heemels. (2015) Design of a Variable Gain Integrator with Reset, In Proc. of the American Control Conference, Chicago, IL, pp. 2155-2160.

[10] S.J.L.M. van Loon, K.G.J. Gruntjens, M.F. Heertjes, N. van de Wouw, and W.P.M.H. Heemels. (2017) Frequency-domain tools for stability analysis of reset control systems, Automatica, 82, pp. 101-108.

[11] R. Ortega, A. Loria, and R. Kelly. (1995) A semiglobally stable output feedback PI^{2}D regulator for robot manipulators, IEEE Trans. on Automatic Control, 40(8), pp. 1432-1436.

[12] L. Zaccarian, D. Nešić, and A.R. Teel. (2010) Analytical and numerical Lyapunov functions for SISO linear control systems with first-order reset elements, Int. J. of Robust & Nonlinear Control, 21(10), pp. 1134-1158.